Anisotropic optical properties of detwinned $BaFe_2As_2$

Christopher C. Homes [1,*] Thomas Wolf,[2] and Christoph Meingast[2,†]

[1]*Condensed Matter Physics and Materials Science Division, Brookhaven National Laboratory, Upton, New York 11973, USA*

[2]*Institute for Quantum Materials and Technologies, Karlsruhe Institute of Technology, 76021 Karlsruhe, Germany*

(Received 3 July 2020; accepted 30 September 2020; published 23 October 2020)

The optical properties of a large, detwinned single crystal of $BaFe_2As_2$ have been examined over a wide frequency range above and below the structural and magnetic transition at $T_N \simeq 138$ K. Above T_N the real part of the optical conductivity and the two infrared-active lattice modes are almost completely isotropic; the lattice modes show a weak polarization dependence just above T_N. For $T < T_N$, the optical conductivity due to the free-carrier response is anisotropic, being larger along the a axis than the b axis below $\simeq$30 meV; above this energy the optical conductivity is dominated by the interband contributions, which appear to be isotropic. The splitting of the low-energy infrared-active mode below T_N is clearly observed, and the polarization modulation of the new modes may be used to estimate that the crystal is $\simeq 70\%$ detwinned. The high-frequency mode, with a threefold increase in strength of the lower branch below T_N and the nearly silent upper branch, remains enigmatic.

DOI: 10.1103/PhysRevB.102.155135

I. INTRODUCTION

In the pantheon of iron-based superconductors, the $AeFe_2As_2$ ("122") materials, where Ae = Ca, Sr, or Ba, are of particular importance because of the many ways in which superconductivity may be induced [1–15]. At room temperature they are paramagnetic metals, but as the temperature is reduced they undergo a structural transition from a tetragonal ($I4/mmm$) to an orthorhombic ($Fmmm$) unit cell, which is accompanied by a magnetic transition and the formation of spin-density-wave-like (SDW) order where the moments are aligned in the a-b planes; ferromagnetically along the b axis, and antiferromagnetically along the a axis. In the case of $BaFe_2As_2$, this transition occurs at $T_N \simeq 138$ K [16]. In the orthorhombic phase, the crystals are heavily twinned. Early optical studies of the in-plane optical properties of $BaFe_2As_2$ examined the average of both orientations in the SDW state [17–19]; however, the application of uniaxial stress along the (110) direction for the tetragonal unit cell results in a nearly twin-free sample [20,21]. Transport [22,23], as well as optical measurements [24–26], of detwinned samples below T_N reveal an anisotropic response where the resistivity along the antiferromagnetic (AFM) direction is lower than that along the ferromagnetic (FM) direction. This is a counterintuitive result as one would normally expect that the scattering from spin fluctuations would result in a higher resistivity along the AFM direction [22]. On the other hand, this anisotropy is sharply reduced in annealed samples for $T \ll T_N$ [24], and the resistivity is indeed observed to be higher along the AFM direction in the related material FeTe below T_N, a result attributed to Hund's rule coupling making transport along the FM direction easier than along the AFM direction [27]. While the designs of the clamped cells used to mechanically detwin single crystals for optical studies are quite elegant [24,25], this approach necessarily requires that the size of the imaging spot is smaller than the crystal, leading to a reduced signal and limiting the ability to track weak spectral features such as lattice modes.

In this work, we examine the temperature dependence of the optical properties of a large single crystal of $BaFe_2As_2$ that has been detwinned through the application of a symmetry-breaking strain, based on differential thermal expansion [28]. While previous studies of detwinned $BaFe_2As_2$ have been performed [24–26], the current study employs the overfilling technique [29] whereby the entire crystal face may be examined, allowing the optical conductivity and the infrared-active modes to be studied. The optical conductivity is essentially isotropic for $T > T_N$. The relatively large size of the sample allows the two normally infrared-active modes above T_N to be identified; the lattice modes show a slight polarization dependence just above T_N in response to the applied strain. For $T < T_N$ the optical conductivity due to the free-carrier response is anisotropic and is higher along the a direction, in agreement with previous work. Interestingly, the interband contributions appear to be isotropic. Below T_N the degeneracy of the infrared-active vibrations is lifted and they split into two new modes that are optically active along either the a or b axis; by examining the polarization modulation of the low-frequency modes below T_N, it is possible to estimate that the sample is about 70% detwinned. The behavior of the high-frequency mode is very curious, with one branch increasing dramatically in strength, while the other remains largely silent. This technique for detwinning crystals may in principle be used to allow further detailed optical studies of, e.g., the $Ba(Fe_{1-x}Co_x)_2As_2$ family of materials.

*homes@bnl.gov

†christoph.meingast@kit.edu

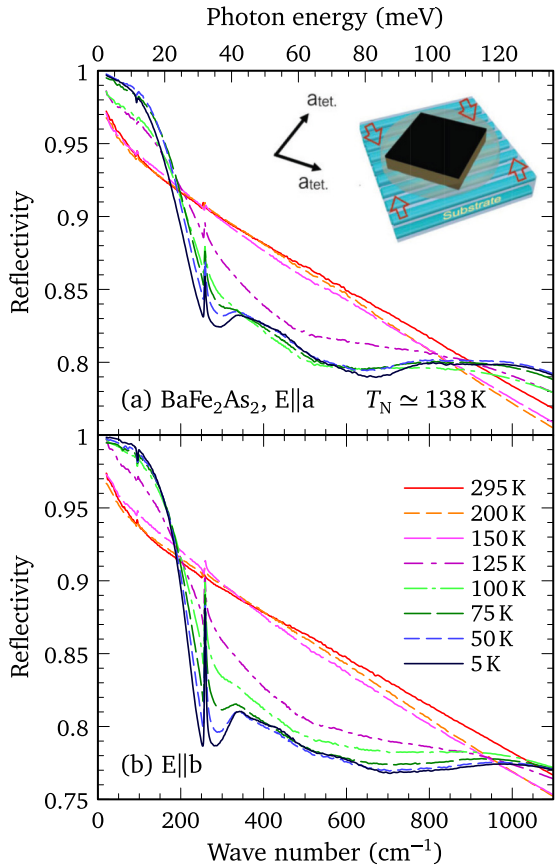

FIG. 1. The reflectivity in the infrared region for a single crystal of $BaFe_2As_2$ at several temperatures above and below $T_N \simeq 138$ K for light polarized along (a) the a axis and (b) the b axis. The resolution at low frequency is typically better than 2 cm^{-1}. The inset shows the orientation of the GFRP with respect to the tetragonal unit cell.

II. EXPERIMENT

Large single crystals of $BaFe_2As_2$ were grown by a self-flux method [28]. The crystals have well-defined growth faces, allowing the a axis in the tetragonal phase to be identified. A piece of thin glass-fiber reinforced plastic (GFRP) $\simeq 0.5$ mm thick was cut and shaped to match a crystal approximately 2 mm $\times$ 2 mm and $\simeq$100 μm thick, and attached using epoxy with the fibers oriented along the (110) direction in the tetragonal phase, shown in the inset of Fig. 1(a). It has been demonstrated that the difference of the thermal expansion parallel and perpendicular to the fiber direction of the GFRP substrate is comparable to the orthorhombic distortion in $BaFe_2As_2$ near T_N, resulting in a large symmetry breaking strain; this technique has been used successfully to measure the resistivity and susceptibility anisotropies in $BaFe_2As_2$ (results and experimental details regarding this method of detwinning may be found in Ref. [28]). The entire arrangement was glued to the tip of an optically black cone. The temperature dependence of the reflectivity has been measured above and below T_N over a wide frequency range (2 meV to over 3 eV) using an overfilling technique in combination with *in situ* evaporation [29]; the results are shown in the infrared region in Figs. 1(a) and 1(b) for light polarized along the a and b axes in the orthorhombic phase, respectively. Above T_N the reflectivity along the two polarizations is nearly identical; only the reflectivity at 150 K along the b axis appears to be slightly higher than its counterpart along the a axis. Below T_N the optical properties are strongly anisotropic. A plasmalike edge develops in the reflectivity for both polarizations. For $T \ll T_N$ the low-frequency reflectivity approaches unity, while above $\simeq$20 meV the reflectivity decreases rapidly before forming a plateau above $\simeq$50 meV; however, the reflectivity levels and the width of the plasmalike edge are very different along the a and b directions, in agreement with previous optical studies of this material [24–26]. Additional structure is observed in the midinfrared region up to about 0.5 eV, above which the reflectivity is comparable to the room-temperature values and displays little temperature dependence (the temperature dependence of the reflectivity is shown over a wide range in Fig. S1 of the Supplemental Material [30]). Superimposed upon the reflectance are two sharp features attributed to the infrared-active lattice modes at $\simeq$95 and 256 cm^{-1} [31], which display an anisotropic response below T_N.

While the reflectance is a useful quantity, it is a combination of the real and imaginary parts of the dielectric function, and as such it is not an intuitive quantity. The complex dielectric function, $\tilde{\epsilon}(\omega) = \epsilon_1 + i\epsilon_2$, has been determined from a Kramers-Kronig analysis of the reflectivity. At low frequency, a metallic Hagen-Rubens extrapolation, $R(\omega) = 1 - A\sqrt{\omega}$, was employed, where A is chosen to match the value of the reflectance at the lowest measured frequency. Above the highest measured frequency point, the reflectance was assumed to be constant to 8×10^4 cm^{-1}, above which a free-electron approximation ($R \propto \omega^{-4}$) was assumed [32].

III. RESULTS AND DISCUSSION

The temperature dependence of the real part of the optical conductivity is shown for light polarized along the a and b axes in Figs. 2(a) and 2(b), respectively. Above T_N the real parts of the optical conductivity for the two polarizations are almost identical; however, below T_N, there is a remarkable anisotropy below $\simeq$300 cm^{-1} where the conductivity along the a direction is larger than along b, in agreement with other studies [24–26]. In addition to the broad features associated with the free-carrier response and the interband excitations, there are narrow lattice modes that also display an anisotropic response. The behavior of the electronic properties will be examined first, followed by the lattice modes.

A. Electronic response

The optical properties of this multiband material have been studied extensively in the twinned materials, and they are described by a Drude-Lorentz model in which at least two different contributions to the free-carrier response are considered [33], resulting in the complex dielectric function

$$\tilde{\epsilon}(\omega) = \epsilon_\infty - \sum_j \frac{\omega_{p,D;j}^2}{\omega^2 + i\omega/\tau_{D,j}} + \sum_k \frac{\Omega_k^2}{\omega_k^2 - \omega^2 - i\omega\gamma_k}, \quad (1)$$

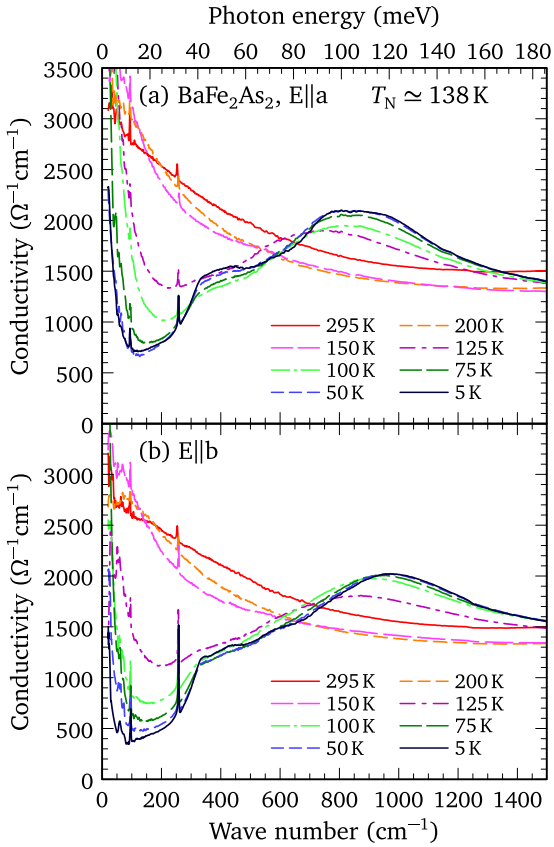

FIG. 2. The temperature dependence of the real part of the optical conductivity of $BaFe_2As_2$ above and below T_N for light polarized along (a) the a axis and (b) the b axis.

where ϵ_∞ is the real part of the dielectric function at high frequency, and $\omega^2_{p,D;j} = 4\pi ne^2/m^*$ and $1/\tau_{D,j}$ are the plasma frequency and scattering rate for the delocalized (Drude) carriers for the jth band, respectively; ω_k, γ_k, and Ω_k are the position, width, and oscillator strength of the kth vibration or bound excitation (the intensity is proportional to Ω_k^2). The complex conductivity, $\tilde{\sigma}(\omega)$, is calculated from the complex dielectric function, $\tilde{\sigma}(\omega) = \sigma_1 + i\sigma_2 = -2\pi i\omega[\tilde{\epsilon}(\omega) - \epsilon_\infty]/Z_0$, where $Z_0 \simeq 377\ \Omega$ is the impedance of free space. The real and imaginary parts of the complex conductivity have been fit simultaneously to Eq. (1) using a nonlinear least-squares technique.

Above T_N, the reflectivity and the optical conductivity show little polarization dependence. Although the features are rather broad, just above T_N at 150 K, the fits to the optical conductivity yield a narrow Drude component ($D1$), $\omega_{p,D1} \simeq 4100\ \text{cm}^{-1}$ and $1/\tau_{D1} \simeq 130\ \text{cm}^{-1}$, and a broad Drude term ($D2$), $\omega_{p,D2} \simeq 11\,900\ \text{cm}^{-1}$ and $1/\tau_{D2} \simeq 1300\ \text{cm}^{-1}$ (Table I), in good agreement with the values from a previous study [34].

Below the structural and magnetic transition at T_N, the optical conductivity undergoes significant changes, shown in Figs. 1 and 2, due to the reconstruction of the Fermi surface [35]. The fits for $T \ll T_N$ at 5 K for the a and b polarizations are shown in Figs. 3(a) and 3(b), respectively, where they have been decomposed into the individual contributions from the various Drude and Lorentz components. The observed optical anisotropy of $\sigma_{1,a}/\sigma_{1,b} \simeq 2$ in the far-infrared region is in good agreement with another study that employed a mechanical apparatus to detwin the crystal [24]. As in the twinned materials, below T_N new features appear at $\simeq$350 and 900 cm^{-1} [34]; interestingly, there appears to be little or no anisotropy in either these or other bound excitations associated with the interband transitions in this compound. Indeed, the oscillator parameters for the bound excitations in Figs. 3(a) and 3(b) are nearly identical for both polarizations, and they are similar to what is observed in the twinned material. The anisotropy in the far-infrared region of the optical conductivity arises purely from the behavior of the free carriers.

As in the case of the twinned materials, for $T \ll T_N$ the plasma frequency for the narrow Drude component undergoes only a small decrease, while the scattering rate drops precipitously: along the a axis, $\omega_{p,D1} \simeq 3500\ \text{cm}^{-1}$ and $1/\tau_{D1} \simeq 3.6\ \text{cm}^{-1}$; along the b axis, $\omega_{p,D1} \simeq 3700\ \text{cm}^{-1}$ and $1/\tau_{D1} \simeq 2.1\ \text{cm}^{-1}$. The uncertainties associated with the small scattering rates, and the similarity of the plasma frequencies, suggest that the narrow Drude component is fairly isotropic below T_N. The plasma frequency for the broad Drude component decreases significantly, while the change in the scattering rate, while significant, is not as dramatic as it is for the narrow Drude component: along the a axis, $\omega_{p,D2} \simeq 2900\ \text{cm}^{-1}$ and $1/\tau_{D2} \simeq 146\ \text{cm}^{-1}$; along the b axis, $\omega_{p,D2} \simeq 2100\ \text{cm}^{-1}$ and $1/\tau_{D2} \simeq 210\ \text{cm}^{-1}$ (Table I). The large difference in the plasma frequencies arises from a smaller effective mass along the a axis where the SDW is present, suggesting a decrease in the electronic correlations [36,37], as opposed to the b axis, or FM direction, where the larger effective mass significantly reduces the plasma frequency and subsequent contribution to the optical conductivity in the far-infrared region.

TABLE I. The plasma frequencies and scattering rates of the narrow ($D1$) and broad ($D2$) Drude terms, as well as several Lorentzian components, returned from the fits to the real and imaginary parts of the optical conductivity for $BaFe_2As_2$ for light polarized in the a-b planes at $T \gtrsim T_N$, and for light polarized along the a and b axes at $T \ll T_N$. All units are in cm^{-1}.

Pol.	Temperature	Component	ω_k	$1/\tau_D$, γ_k	$\omega_{p,D}$, Ω_k
$E \parallel ab$	($T \simeq T_N$)	$D1$		130	4110
		$D2$		1346	11 900
		LM	4052	6110	23 004
$E \parallel a$	($T \ll T_N$)	$D1$		3.6	3450
		$D2$		146	2910
		$L1$	361	293	3900
		$L2$	861	989	10196
		LM	4154	6500	24036
$E \parallel b$	($T \ll T_N$)	$D1$		2.1	3690
		$D2$		207	2080
		$L1$	387	326	3900
		$L2$	953	1110	10382
		LM	4012	6258	24584

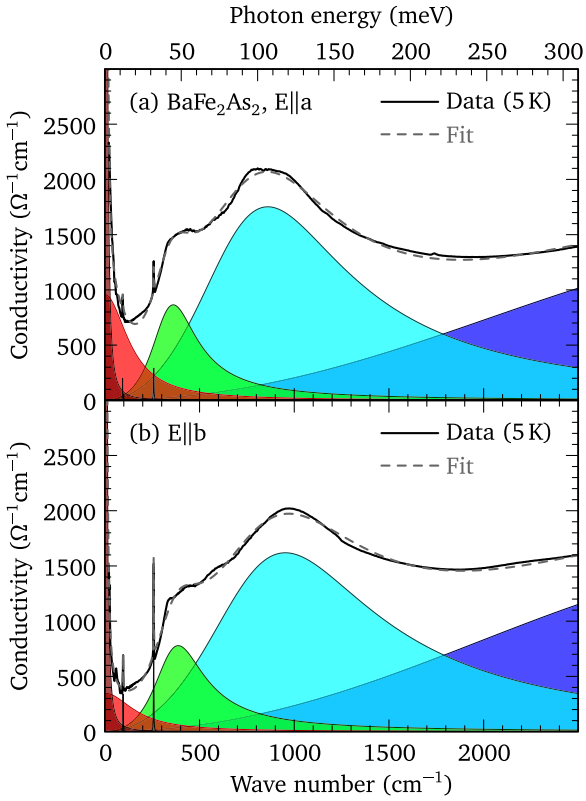

FIG. 3. The results of the fits to the complex conductivity of $BaFe_2As_2$ below T_N at 5 K compared to the real part of the optical conductivity in the far- and midinfrared regions for light polarized along (a) the a axis and (b) the b axis. The anisotropic response is strongest below $\simeq$30 meV. The fit is decomposed into the contributions from the narrow and broad Drude components, as well as several Lorentz oscillators (Table I).

B. Lattice modes

In the high-temperature tetragonal phase, the irreducible vibrational representation for the infrared modes yields $2A_{2u} + 2E_u$ vibrations [38], where the singly degenerate A_{2u} modes are active along the c axis, and the doubly degenerate E_u modes are active in the planes. Below the tetragonal to orthorhombic structural transition at T_N, the degeneracy of the in-plane modes is lifted, $E_u \rightarrow B_{2u} + B_{3u}$, where the B_{2u} and B_{3u} modes are active along the b and a axes, respectively. In the twinned samples, the low-frequency E_u mode observed at $\simeq$94 cm^{-1} above T_N involves the in-plane displacements of the Ba atom moving in opposition to the Fe and As atoms; below T_N this mode splits into two features at $\simeq$93 and 96 cm^{-1} [39]. The high-frequency mode at $\simeq$256 cm^{-1} does not appear to split below T_N, instead displaying an anomalous increase in oscillator strength [18]; this mode involves only the in-plane displacements of Fe and As atoms which move in opposition to one and other [31,40]. In the detwinned samples, the low-frequency mode has not been examined; the high-frequency mode displays the same anomalous increase in oscillator strength below T_N, but it also does not appear to split and is active only along the b axis [24]. In this work, we are able to examine the splitting and the polarization dependence of the low-frequency E_u mode below T_N, as well as the details of the high-frequency mode.

1. Low-frequency mode

The low-frequency E_u mode has been fit using the Lorentzian oscillator described in Eq. (1) superimposed on a linear background. Above T_N at 295 K, this mode is almost completely isotropic, with $\omega_0 \simeq 93.7$, $\gamma_0 \simeq 2.5$, and $\Omega_0 \simeq 195$ cm^{-1}. (Asymmetric line shapes were also considered in the Supplemental Material [30], but the asymmetry parameter was quite small, effectively resulting in a symmetric Lorentzian oscillator.) Interestingly, just above T_N at 150 K there is a slight polarization dependence with $\omega_0 \simeq 94$ cm^{-1} along the a axis and $\omega_0 \simeq 95$ cm^{-1} along the b axis, while the width and strength show no such dependence. This indicates that GFRP is imparting some strain on the crystal and creating a slight asymmetry just above T_N. This is consistent with the observation of a significant anisotropy in the resistivity just above T_N, which was attributed to the magnetic transition rather than nematic fluctuations [28]. Similarly, the vibrational splitting just above the transition would suggest that the phonons are coupling to the magnetism. Below T_N this vibration clearly splits into two modes at $\simeq$94 and 96 cm^{-1} at low temperature, both of which display a strong polarization dependence. The optical conductivity is shown in the region of the low-frequency B_{3u} and B_{2u} modes at 5 K for light polarized along the a and b axis in Figs. 4(a) and 4(b), respectively; the different contributions are denoted in the legend, while the fitted oscillator parameters are shown in the panels of Fig. 4. While the two modes display a strong polarization dependence, the modulation is not perfect. The polarization modulation of the oscillators may be used to estimate the degree to which the crystal is detwinned in the following way:

$$\alpha_j = 1 - \frac{\Omega_j^2(\perp)}{\Omega_j^2(\parallel)}, \tag{2}$$

where $\perp$ and $\parallel$ denote the polarizations perpendicular and parallel to the dipole moment of the jth vibration. In the case of a twinned crystal, there is no polarization dependence, $\Omega_j(\perp) = \Omega_j(\parallel)$, and $\alpha_j = 0$; if the crystal is completely detwinned, then $\Omega_j(\perp) = 0$ and $\alpha_j = 1$. Using the parameters for the B_{2u} mode at 5 K yields $\alpha \simeq 0.72$; the average for the two modes of $\alpha \simeq 0.7$ indicates that the crystal is roughly 70% twin-free, which is comparable to the estimate of $\sim$80% based on transport measurements [28]. We speculate that by gluing the GFRP and sample arrangement to an optical mount, the strain imparted on the sample may be slightly reduced, resulting in the slightly lower degree of detwinning observed in this work.

2. High-frequency mode

The high-frequency E_u mode is of considerable interest as one branch displays an anomalous increase in oscillator strength below T_N [18], while the other appears to be largely silent [24]. The high-frequency mode has been fit using a simple Lorentzian oscillator superimposed on a polynomial background; the resulting line shapes are shown with the background removed for light polarized along the a and b

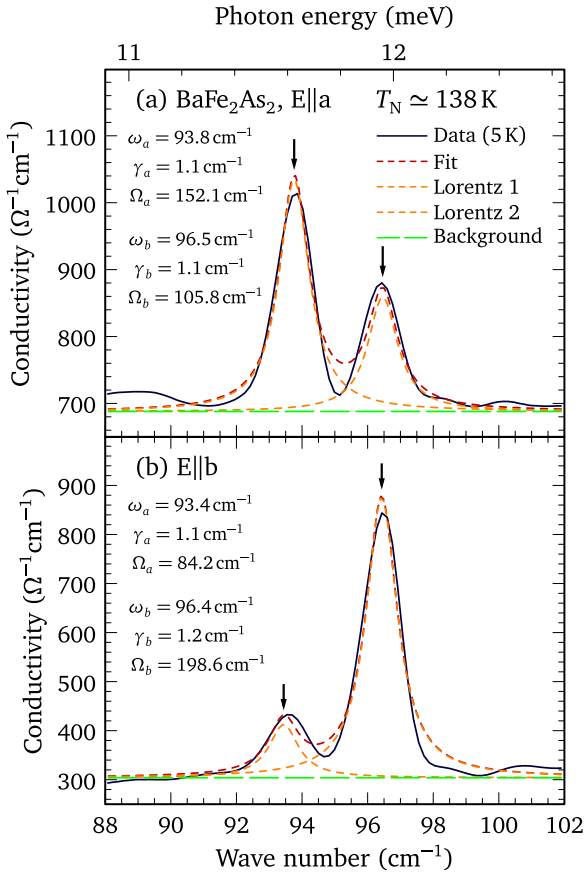

FIG. 4. The real part of the optical conductivity of $BaFe_2As_2$ in the orthorhombic phase at 5 K in the region of the low-frequency B_{3u} and B_{2u} modes with an experimental resolution of 1 cm^{-1} for light polarized along (a) the a axis and (b) the b axis. For each polarization, the vibrational structure has been fit to two Lorentz oscillators superimposed on a linear background. The fitted oscillator parameters are listed in each panel; the positions are indicated by the arrows.

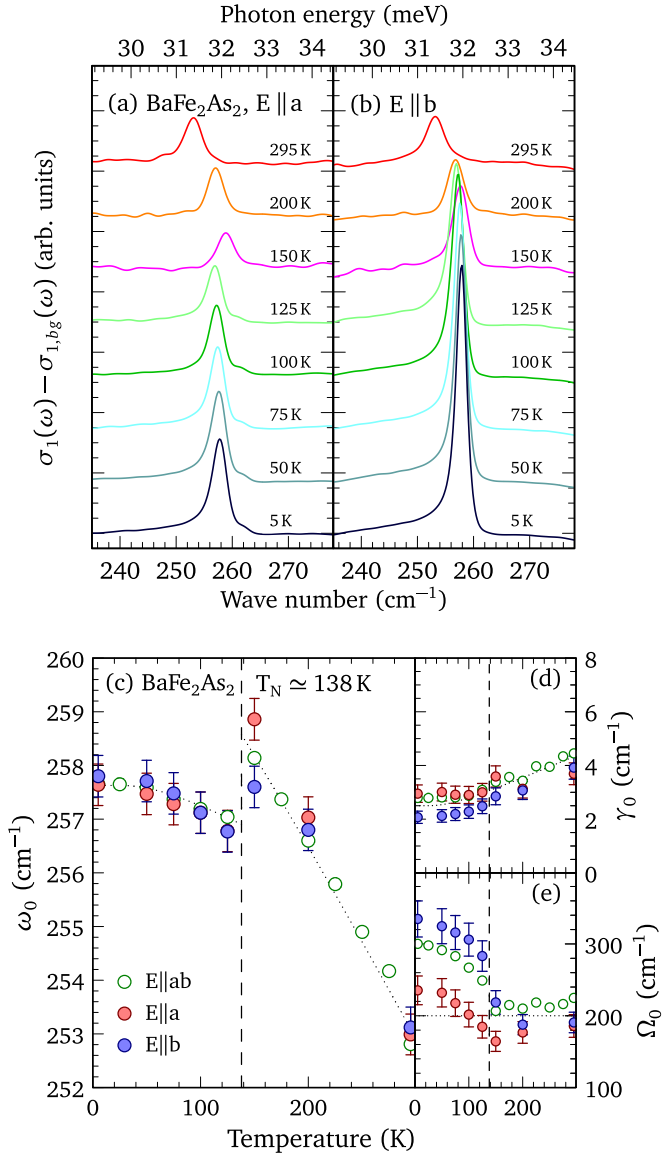

FIG. 5. The temperature dependence of the real part of the optical conductivity in the region of the high-frequency B_{3u} and B_{2u} modes with the electronic background removed for light polarized (a) along the a axis and (b) along the b axis; offsets have been added for clarity. The temperature dependence of the (c) position, (d) width, and (e) strength of the lattice mode in a twinned sample [31], compared to the polarized results determined in this work.

axes in Figs. 5(a) and 5(b), respectively. The line shape for this oscillator at 5 K has an asymmetric line shape, suggesting electron-phonon coupling; while an asymmetric Fano line shape has been fit to this vibration, the asymmetry parameter is very small [31] (see Fig. S3 and the accompanying table). The results for the position, width, and strength of the oscillators along the a and b axes are shown in Figs. 5(c), 5(d), and 5(e), respectively, where they are compared with results from a twinned sample ($E \parallel ab$) [31]. Above 200 K there is no polarization dependence in the oscillator parameters for this mode; however, in a reversal of the behavior observed in the low-frequency E_u mode, just above T_N at 150 K the position of this mode for light polarized along what will become the a axis is slightly larger than it is along the b axis, again indicating that just above T_N the strain from the GFRP is a symmetry-breaking process and that the lattice modes are likely coupling to the magnetism. The frequency of this mode appears to decrease anomalously below T_N; this is understood as the splitting of the E_u mode where the lower B_{2u} branch is active and the upper B_{3u} branch is largely silent [31]. The fact that the positions of the modes along the a and b axes are identical [Fig. 5(c)] suggests that the activity of the mode along the a axis is likely due to leakage from the b axis as a result of residual twins, and that the weak shoulder observed just above this mode at $\simeq 261$ cm^{-1} [Fig. 5(a) and supplemental Fig. S3(a)] is the B_{3u} mode [39]. The oscillator strength of the B_{2u} mode was observed to increase by a factor of 2 in the twinned material [18], but in the largely twin-free sample it has increased threefold, in agreement with a previous study [24]. The origin of this anomalous increase in the strength remains a topic of considerable debate. Given the value of $\alpha \simeq 0.7$ determined from the modulation of the low-frequency E_u mode, and the value of $\Omega_0(\parallel) \simeq 340$ cm^{-1} for the b-axis mode at 5 K, the strength of the leakage should

be $\Omega_0(\perp) \simeq 186$ cm^{-1}; curiously, the observed value of $\Omega_0(\perp) \simeq 235$ cm^{-1} is considerably larger and suggests a lower value for the detwinning. However, the rather peculiar nature of this mode makes it a poor candidate for estimates of the degree of detwinning. The more predictable behavior of the low-frequency B_{2u} and B_{3u} modes suggests that the estimate of $\simeq$70% detwinning is the more reliable one.

IV. CONCLUSIONS

The optical properties of a large, detwinned single crystal of $BaFe_2As_2$ have been determined above and below $T_N \simeq 138$ K over a wide frequency range. Above T_N the optical conductivity and the two infrared-active E_u modes are essentially isotropic; only the lattice modes display a weak polarization dependence just above T_N. Below T_N, the free-carrier response is strongly anisotropic; below $\simeq$30 meV, $\sigma_{1,a}/\sigma_{1,b} \sim 2$. The narrow Drude component has only a weak polarization dependence. The anisotropy in the low-energy optical conductivity is driven by the difference in the effective masses in the broad Drude component. The interband contributions to the optical conductivity above this energy appear to be isotropic. The relatively large sample size allows the behavior of the lattice modes to be studied in detail. The splitting of the low-energy E_u mode is clearly observed, and the polarization modulations of the resulting B_{2u} and B_{3u} modes are used to determine that the crystal is about 70% detwinned. The high-frequency mode remains enigmatic; the B_{2u} component undergoes a striking threefold increase in intensity, while the B_{3u} mode is nearly silent. This relatively simple method for detwinning crystals may allow further detailed optical studies of the nematic and (or) superconducting behavior in this family of materials.

ACKNOWLEDGMENTS

We would like to acknowledge useful discussions with Ana Akrap and Mingquan He. Work at Brookhaven National Laboratory was supported by the Office of Science, U.S. Department of Energy under Contract No. DE-SC0012704. Work at KIT was partially funded by the Deutsche Forschungsgemeinschaft (DFG, German Research Foundation) - TRR 288-422213477 (project A2).

[1] M. Rotter, M. Tegel, and D. Johrendt, Superconductivity at 38 K in the Iron Arsenide $(Ba_{1-x}K_x)Fe_2As_2$, Phys. Rev. Lett. **101**, 107006 (2008).

[2] A. S. Sefat, R. Jin, M. A. McGuire, B. C. Sales, D. J. Singh, and D. Mandrus, Superconductivity at 22 K in Co-Doped $BaFe_2As_2$ Crystals, Phys. Rev. Lett. **101**, 117004 (2008).

[3] N. Ni, M. E. Tillman, J.-Q. Yan, A. Kracher, S. T. Hannahs, S. L. Bud'ko, and P. C. Canfield, Effects of Co substitution on thermodynamic and transport properties and anisotropic H_{c2} in $Ba(Fe_{1-x}Co_x)_2As_2$ single crystals, Phys. Rev. B **78**, 214515 (2008).

[4] K. Sasmal, B. Lv, B. Lorenz, A. M. Guloy, F. Chen, Y.-Y. Xue, and C.-W. Chu, Superconducting Fe-Based Compounds $(A_{1-x}Sr_x)Fe_2As_2$ with $A =$ K and Cs with Transition Temperatures up to 37 K, Phys. Rev. Lett. **101**, 107007 (2008).

[5] G.-F. Chen, Z. Li, G. Li, W.-Z. Hu, J. Dong, X.-D. Z. Jun Zhou, P. Zheng, N.-L. Wang, and J.-L. Luo, Superconductivity in hole-doped $(Sr_{1-x}K_x)Fe_2As_2$, Chin. Phys. Lett. **25**, 3403 (2008).

[6] P. L. Alireza, Y. T. C. Ko, J. Gillett, C. M. Petrone, J. M. Cole, G. G. Lonzarich, and S. E. Sebastian, Superconductivity up to 29 K in $SrFe_2As_2$ and $BaFe_2As_2$ at high pressures, J. Phys.: Condens. Matter **21**, 012208 (2008).

[7] J.-H. Chu, J. G. Analytis, C. Kucharczyk, and I. R. Fisher, Determination of the phase diagram of the electron-doped superconductor $Ba(Fe_{1-x}Co_x)_2As_2$, Phys. Rev. B **79**, 014506 (2009).

[8] T. Goko, A. A. Aczel, E. Baggio-Saitovitch, S. L. Bud'ko, P. C. Canfield, J. P. Carlo, G. F. Chen, P. Dai, A. C. Hamann, W. Z. Hu, H. Kageyama, G. M. Luke, J. L. Luo, B. Nachumi, N. Ni, D. Reznik, D. R. Sanchez-Candela, A. T. Savici, K. J. Sikes, N. L. Wang, C. R. Wiebe, T. J. Williams, T. Yamamoto, W. Yu, and Y. J. Uemura, Superconducting state coexisting with a phase-separated static magnetic order in (Ba, K)Fe_2As_2, (Sr, Na)Fe_2As_2, and $CaFe_2As_2$, Phys. Rev. B **80**, 024508 (2009).

[9] S. R. Saha, N. P. Butch, K. Kirshenbaum, and J. Paglione, Evolution of bulk superconductivity in $SrFe_2As_2$ with Ni substitution, Phys. Rev. B **79**, 224519 (2009).

[10] S. Jiang, H. Xing, G. Xuan, C. Wang, Z. Ren, C. Feng, J. Dai, Z. Xu, and G. Cao, Superconductivity up to 30 K in the vicinity of the quantum critical point in $BaFe_2(As_{1-x}P_x)_2$, J. Phys.: Condens. Matter **21**, 382203 (2009).

[11] H. L. Shi, H. X. Yang, H. F. Tian, J. B. Lu, Z. W. Wang, Y. B. Qin, Y. J. Song, and J. Q. Li, Structural properties and superconductivity of $SrFe_2As_{2-x}P_x$ and $(0.0 \leqslant x \leqslant 1.0)$ and $CaFe_2As_{2-y}P_y$ $(0.0 \leqslant y \leqslant 0.3)$, J. Phys.: Condens. Matter **22**, 125702 (2010).

[12] R. Cortes-Gil and S. J. Clarke, Structure, magnetism, and superconductivity of the layered iron arsenides $Sr_{1-x}Na_xFe_2As_2$, Chem. Mater. **23**, 1009 (2011).

[13] F. Ishikawa, N. Eguchi, M. Kodama, K. Fujimaki, M. Einaga, A. Ohmura, A. Nakayama, A. Mitsuda, and Y. Yamada, Zero-resistance superconducting phase in $BaFe_2As_2$ under high pressure, Phys. Rev. B **79**, 172506 (2009).

[14] E. Colombier, S. L. Bud'ko, N. Ni, and P. C. Canfield, Complete pressure-dependent phase diagrams for $SrFe_2As_2$ and $BaFe_2As_2$, Phys. Rev. B **79**, 224518 (2009).

[15] K. Kitagawa, N. Katayama, H. Gotou, T. Yagi, K. Ohgushi, T. Matsumoto, Y. Uwatoko, and M. Takigawa, Spontaneous Formation of a Superconducting and Antiferromagnetic Hybrid State in $SrFe_2As_2$ Under High Pressure, Phys. Rev. Lett. **103**, 257002 (2009).

[16] M. Rotter, M. Tegel, D. Johrendt, I. Schellenberg, W. Hermes, and R. Pöttgen, Spin-density-wave anomaly at 140 K in the ternary iron arsenide $BaFe_2As_2$, Phys. Rev. B **78**, 020503(R) (2008).

[17] W. Z. Hu, J. Dong, G. Li, Z. Li, P. Zheng, G. F. Chen, J. L. Luo, and N. L. Wang, Origin of the Spin Density Wave Instability

in AFe_2As_2 (A = Ba, Sr) as Revealed by Optical Spectroscopy, Phys. Rev. Lett. **101**, 257005 (2008).

[18] A. Akrap, J. J. Tu, L. J. Li, G. H. Cao, Z. A. Xu, and C. C. Homes, Infrared phonon anomaly in $BaFe_2As_2$, Phys. Rev. B **80**, 180502(R) (2009).

[19] F. Pfuner, J. G. Analytis, J.-H. Chu, I. R. Fisher, and L. Degiorgi, Charge dynamics of the spin-density-wave state in $BaFe_2As_2$, Eur. Phys. J. B **67**, 513 (2009).

[20] M. A. Tanatar, A. Kreyssig, S. Nandi, N. Ni, S. L. Bud'ko, P. C. Canfield, A. I. Goldman, and R. Prozorov, Direct imaging of the structural domains in the iron pnictides AFe_2As_2(A = Ca, Sr, Ba), Phys. Rev. B **79**, 180508(R) (2009).

[21] I. R. Fisher, L. Degiorgi, and Z. X. Shen, In-plane electronic anisotropy of underdoped '122' Fe-arsenide superconductors revealed by measurements of detwinned single crystals, Rep. Prog. Phys. **74**, 124506 (2011).

[22] J.-H. Chu, J. G. Analytis, K. De Greve, P. L. McMahon, Z. Islam, Y. Yamamoto, and I. R. Fisher, In-plane resistivity anisotropy in an underdoped iron arsenide superconductor, Science **329**, 824 (2010).

[23] T. Kissikov, R. Sarkar, M. Lawson, B. T. Bush, E. I. Timmons, M. A. Tanatar, R. Prozorov, S. L. Bud'ko, P. C. Canfield, R. M. Fernandes, and N. J. Curro, Uniaxial strain control of spin-polarization in multicomponent nematic order of $BaFe_2As_2$, Nat. Commun. **9**, 1058 (2018).

[24] M. Nakajima, T. Liang, S. Ishida, Y. Tomioka, K. Kihou, C. H. Lee, A. Iyo, H. Eisaki, T. Kakeshita, T. Ito, and S. Uchida, Unprecedented anisotropic metallic state in undoped iron arsenide $BaFe_2As_2$ revealed by optical spectroscopy, Proc. Natl. Acad. Sci. (USA) **108**, 12238 (2011).

[25] A. Dusza, A. Lucarelli, A. Sanna, S. Massidda, J.-H. Chu, I. R. Fisher, and L. Degiorgi, Anisotropic in-plane optical conductivity in detwinned $Ba(Fe_{1-x}Co_x)_2As_2$, New J. Phys. **14**, 023020 (2012).

[26] C. Mirri, A. Dusza, S. Bastelberger, M. Chinotti, L. Degiorgi, J.-H. Chu, H.-H. Kuo, and I. R. Fisher, Origin of the Resistive Anisotropy in the Electronic Nematic Phase of $BaFe_2As_2$ Revealed by Optical Spectroscopy, Phys. Rev. Lett. **115**, 107001 (2015).

[27] J. Jiang, C. He, Y. Zhang, M. Xu, Q. Q. Ge, Z. R. Ye, F. Chen, B. P. Xie, and D. L. Feng, Distinct in-plane resistivity anisotropy in a detwinned FeTe single crystal: Evidence for a Hund's metal, Phys. Rev. B **88**, 115130 (2013).

[28] M. He, L. Wang, F. Ahn, F. Hardy, T. Wolf, P. Adelmann, J. Schmalian, I. Eremin, and C. Meingast, Dichotomy between in-plane magnetic susceptibility and resistivity anisotropies in extremely strained $BaFe_2As_2$, Nat. Commun. **8**, 504 (2017).

[29] C. C. Homes, M. Reedyk, D. A. Crandles, and T. Timusk, Technique for measuring the reflectance of irregular, submillimeter-sized samples, Appl. Opt. **32**, 2976 (1993).

[30] See Supplemental Material at http://link.aps.org/supplemental/10.1103/PhysRevB.102.155135 for the experimental reflectivity and real part of the optical conductivity shown over a wide frequency range, as well as fits of the high-frequency infrared-active mode to an asymmetric Fano line shape, which includes Refs. [41,42].

[31] C. C. Homes, Y. M. Dai, A. Akrap, S. L. Bud'ko, and P. C. Canfield, Vibrational anomalies in AFe_2As_2 (A = Ca, Sr, and Ba) single crystals, Phys. Rev. B **98**, 035103 (2018).

[32] F. Wooten, *Optical Properties of Solids* (Academic, New York, 1972), pp. 244–250.

[33] D. Wu, N. Barišić, P. Kallina, A. Faridian, B. Gorshunov, N. Drichko, L. J. Li, X. Lin, G. H. Cao, Z. A. Xu, N. L. Wang, and M. Dressel, Optical investigations of the normal and superconducting states reveal two electronic subsystems in iron pnictides, Phys. Rev. B **81**, 100512(R) (2010).

[34] Y. M. Dai, A. Akrap, S. L. Bud'ko, P. C. Canfield, and C. C. Homes, Optical properties of AFe_2As_2 (A = Ca, Sr, and Ba) single crystals, Phys. Rev. B **94**, 195142 (2016).

[35] P. Richard, K. Nakayama, T. Sato, M. Neupane, Y.-M. Xu, J. H. Bowen, G. F. Chen, J. L. Luo, N. L. Wang, X. Dai, Z. Fang, H. Ding, and T. Takahashi, Observation of Dirac Cone Electronic Dispersion in $BaFe_2As_2$, Phys. Rev. Lett. **104**, 137001 (2010).

[36] Z. P. Yin, K. Haule, and G. Kotliar, Kinetic frustration and the nature of the magnetic and paramagnetic states in iron pnictides and iron chalcogenides, Nat. Mater. **10**, 932 (2011).

[37] Y. M. Dai, A. Akrap, J. Schneeloch, R. D. Zhong, T. S. Liu, G. D. Gu, Q. Li, and C. C. Homes, Spectral weight transfer in strongly correlated $Fe_{1.03}Te$, Phys. Rev. B **90**, 121114(R) (2014).

[38] A. P. Litvinchuk, V. G. Hadjiev, M. N. Iliev, B. Lv, A. M. Guloy, and C. W. Chu, Raman-scattering study of $K_xSr_{1-x}Fe_2As_2$ (x = 0.0, 0.4), Phys. Rev. B **78**, 060503(R) (2008).

[39] A. A. Schafgans, B. C. Pursley, A. D. LaForge, A. S. Sefat, D. Mandrus, and D. N. Basov, Phonon splitting and anomalous enhancement of infrared-active modes in $BaFe_2As_2$, Phys. Rev. B **84**, 052501 (2011).

[40] M. Sandoghchi, H. Khosroabadi, H. Almasi, and M. Akhavan, Electronic and phonon structures of $BaFe_2As_2$ superconductor by ab-initio density functional theory, J. Supercond. Nov. Magn. **26**, 93 (2013).

[41] A. Damascelli, Optical spectroscopy of quantum spin systems, Ph.D. thesis, University of Groningen, 1996, p. 21.

[42] A. Kuzmenko, Software RefFIT, Manual p. 64 (2014).